





# Femtosecond laser direct inscription of 3D photonic devices in Er/Yb-doped oxyfluoride nano-glass ceramics

JAVIER R. VÁZQUEZ DE ALDANA,<sup>1</sup> CAROLINA ROMERO,<sup>1</sup>  JOAQUÍN FERNÁNDEZ,<sup>2</sup>  GIULIO GORNI,<sup>3</sup> MARÍA JESÚS PASCUAL,<sup>3</sup> ALICIA DURAN,<sup>3</sup> AND ROLINDES BALDA<sup>4,5</sup>

<sup>1</sup>*Aplicaciones del Láser y Fotónica, Applied Physics Department, University of Salamanca, Salamanca 37008, Spain*

<sup>2</sup>*Donostia International Physics Center (DIPC), 20018 San Sebastian, Spain*

<sup>3</sup>*Instituto de Cerámica y Vidrio, ICV-CSIC, 28049 Madrid, Spain*

<sup>4</sup>*Applied Physics Department I, School of Engineering, Basque Country University UPV-EHU, 48013 Bilbao, Spain*

<sup>5</sup>*Materials Physics Center CSIC-UPV/EHU, 20018 San Sebastian, Spain*

**Abstract:** The fabrication of optical waveguides by direct femtosecond laser irradiation in Er<sup>3+</sup>/Yb<sup>3+</sup> oxyfluoride nano-glass ceramics is investigated. Following the strategy of single line irradiation, a wide range of laser parameters can be used to obtain single-mode waveguides with nearly-gaussian modal profiles, in the visible and near-infrared. Measured propagation loss is 1.6 dB/cm for the optimum parameters (0.34 μJ/pulse and 20 μm/s scanning velocity), with no annealing after irradiation, and the induced refractive index contrast is Δn~0.006 (at 800 nm). The multi-scan technique is used to gain control of the refractive index profiles thus producing multimodal structures. The active behavior of the waveguides is induced under ~800 nm seeding and the co-propagating guidance of the erbium emission is demonstrated. The integration of photonic elements such as Y-splitters, both in 2D and 3D, as well as Mach-Zehnder interferometers, is also shown. Results demonstrate the optimum behavior of Er<sup>3+</sup>/Yb<sup>3+</sup> oxyfluoride nano-glass ceramics as a host material for the integration of complex active photonic devices by femtosecond laser irradiation in the low repetition rate regime.

© 2020 Optical Society of America under the terms of the [OSA Open Access Publishing Agreement](#)

## 1. Introduction

The use of ultrashort laser pulses for the inscription of optical waveguides in transparent dielectrics has attracted great attention since the first demonstration [1] due to the intrinsic properties of the technique: the fabrication is direct and can be applied to almost any transparent dielectric, it does not require any specific sample preparation and, more remarkably, it allows the implementation of 3D structures [2]. Among the different substrates used for waveguide inscription by femtosecond laser irradiation, glasses have been the most widely studied provided they show excellent optical properties and, moreover, the fabrication is particularly simple: the interaction with the laser creates, in most of the cases, a refractive index increase at the focal volume that, as it is scanned along the sample, may produce an efficient light-confining structure. Depending on the repetition rate of the fabrication laser it can be distinguished between two working regimes [3]: non-thermal, in which there is no neat heat accumulation in the irradiated region (low repetition rate of ~1 kHz or below) and thermal [4], in which the time between pulses is so short that thermal diffusion do not carry the heat away from the focus before the next pulse arrives so that melting is produced (high repetition rate of ~100 kHz or above). Although the properties of the waveguides generated in both regimes are different, both of them have an enormous interest in the development of complex devices for applications such as, for instance, astrophotonics [5], or for the integration of

opto-fluidic elements in lab-on-a-chip devices [6]. In addition to these “passive” applications in which waveguides act as light conducting channels, active devices [7] have been also implemented in doped glasses as light amplifier or waveguide lasers.

Transparent glass-ceramics (GCs) are constituted by crystals of micrometer or nanometer size embedded in a glass matrix, showing intermediate properties between glasses and ceramics: the embedded crystalline phase enhances certain properties of the matrix glass or introduces new properties, making GCs very interesting in photonic applications [8] or laser cooling [9]. Particularly, oxyfluoride nano-glass ceramics containing rare-earth (RE) doped fluoride nanocrystals combine the good mechanical and chemical stabilities of oxide glasses with the low phonon energy of fluoride crystals ( $300\text{--}400\text{ cm}^{-1}$ ), which prevents non-radiative losses by multiphoton relaxation thus being of great interest in the operation of active devices. These glass-ceramics contain fluoride nanocrystals with size between 10 to 40 nm, after an adequate heat treatment of the precursor glass. The RE ions can be incorporated into the nanocrystals in oxyfluoride GCs [10], by means of a diffusion-controlled process, highly dependent on the temperature.

The inscription of waveguides by femtosecond laser irradiation in RE ( $\text{Er}^{3+}$ ) doped oxyfluoride GCs has been demonstrated in the high repetition-rate regime [11]. The inscribed waveguides showed an “W” shape refractive index modification, leading to irregular modal profiles, and then a thermal treatment was applied to reduce the residual stress created in the waveguide. In the present work we analyze the potential of transparent oxyfluoride nano-glass ceramics co-doped with  $\text{Er}^{3+}/\text{Yb}^{3+}$  ions [10,12] for the integration of 3D photonic devices by femtosecond laser inscription. We demonstrate that, operating in the low repetition rate regime, efficient planar and 3D waveguides can be implemented in this material, and no thermal treatment post-fabrication was needed to obtain nearly gaussian intensity profiles. The waveguides were optically characterized, and our results suggest that this target material is an excellent host for the integration of active photonic devices.

The paper is organized as follows. In Section 2 we describe the main experimental techniques and methods utilized along the work, both in the sample preparation and in the waveguide fabrication and characterization. The main results obtained are presented in Section 3. We firstly optimize the laser writing parameters (pulse energy and scanning velocity) and then different Y-splitting structures are implemented. Section 4 is devoted to the conclusions of the work and final remarks.

## 2. Experimental setup and methods

### 2.1. Samples preparation and characterization

Glasses of composition  $55\text{SiO}_2\text{--}20\text{Al}_2\text{O}_3\text{--}15\text{Na}_2\text{O--}10\text{LaF}_3$  (55Si-10La) doped with  $0.5\text{Er}^{3+}\text{--}2\text{Yb}^{3+}$  (mol %) have been prepared by the melt-quenching technique using as raw materials:  $\text{SiO}_2$  (Saint-Gobin 99.6%),  $\text{Al}_2\text{O}_3$  (Panreac),  $\text{Na}_2\text{CO}_3$  (Sigma Aldrich, >99.5%),  $\text{LaF}_3$  (Alfa Aesar, 99.9%),  $\text{ErF}_3$  (Alfa Aesar, 99.99%) and  $\text{YbF}_3$  (Alfa Aesar, 99.99%). The batches were calcined at  $1200\text{ }^\circ\text{C}$  for 2 h, melted at  $1650\text{ }^\circ\text{C}/\text{min}$  for 1.5 h and then quenched onto a brass mould. The batches were melted again for 30 min and then quenched onto a cold brass mould to improve glass homogeneity. An annealing process at  $600\text{ }^\circ\text{C}$  for 30 min was performed on the as made glasses to eliminate residual stresses. Glass-ceramics samples have been obtained upon heat treatments of glass pieces at  $620\text{ }^\circ\text{C--}40\text{ h}$ , using a heating rate of  $10\text{ }^\circ\text{C}/\text{min}$ . Finally, the samples were cut to dimensions of  $\sim 10\times 12\times 3\text{ mm}^3$  and were optically polished.

High resolution electron microscopy (HR-TEM), including Scanning Transmission Microscopy-High Angle Annular Dark Field (STEM-HAADF) were recorded on a JEOL 2100 field emission gun transmission electron microscope, operating at 200 kV and providing a point resolution of 0.19 nm. TEM analysis clearly demonstrates the formation of  $\text{LaF}_3$  nanocrystals in the heat-treated samples. As an example, Fig. 1 shows the micrograph of the glass-ceramic sample

co-doped with  $0.5\text{Er}^{3+}-2\text{Yb}^{3+}$  (mol %) where phase separation droplets are observed. Several crystals grow inside phase separation droplets already present in the starting glass. The mean crystal size is around 11 nm, in agreement with the value obtained from XRD [10], instead the mean droplet size is around 30 nm.

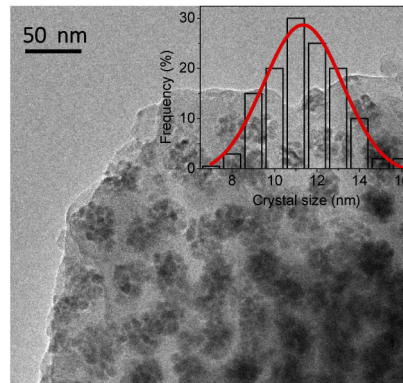


**Fig. 1.** TEM micrograph of glass-ceramic sample codoped with  $0.5\text{Er}^{3+}-2\text{Yb}^{3+}$  (mol %) treated at  $620\text{ }^\circ\text{C}-40\text{ h}$  and its corresponding particle size distribution.

## 2.2. Waveguide fabrication

An amplified femtosecond laser system (Spitfire, Spectra-Physics) was used for the inscription of the 3D optical waveguides in the glass. The laser emitted linearly-polarized pulses with 120 fs duration at a low repetition rate of 1 kHz (non-thermal regime). The central wavelength of the pulse was 795 nm ( $\sim 10$  nm spectral width). The control of the pulse energy was done by using, firstly, a half-wave plate and a linear polarized, and secondly, a calibrated neutral density filter. The sample to be processed was placed in a XYZ micro-positioning stage, and the beam was focused by a  $40\times$  microscope objective (N.A. = 0.65) at a depth of  $\sim 100\text{ }\mu\text{m}$  beneath the sample surface in a transversal writing geometry [13].

The initial study consisted on the inscription of single straight lines at different conditions of pulse energy, from the minimum value at which a slight modification is observed when inspecting the sample with the optical microscope ( $\sim 0.07\text{ }\mu\text{J}$ ) to a value of  $0.68\text{ }\mu\text{J}$  at which severe damage is evident. A wide range of scanning velocities ( $20-250\text{ }\mu\text{m/s}$ ) is also tested for each incident pulse energy. The polarization of the laser was kept perpendicular to the scanning direction. In another set of experiments, we used the multi-scan technique [14] in order to increase the transverse size of the optical waveguides, by performing 4 parallel scans with a lateral separation of  $2\text{ }\mu\text{m}$  between adjacent scans. The same energies as before were used, and scanning velocities of  $50$  and  $250\text{ }\mu\text{m/s}$ .

To analyze the possibility to fabricate stress-induced waveguides [15] in this substrate, pairs of lines were also inscribed with separations of  $15$  and  $20\text{ }\mu\text{m}$ , increasing even further the pulse energy (up to  $1\text{ }\mu\text{J}$ ). Moreover, cladding-type structures [16] were tested, that consisted of parallel tracks with a lateral separation of  $2\text{ }\mu\text{m}$  following a circular geometry with radius of  $10$  and  $15\text{ }\mu\text{m}$ . In these cases, the scanning velocity was taken to be  $250\text{ }\mu\text{m/s}$ , and the pulse energy was varied between  $0.17-0.68\text{ }\mu\text{J}$ .

Finally, complex photonic structures such as  $1\times 2$ ,  $1\times 4$  (2D),  $1\times 4$  (3D) Y-splitters, and Mach-Zehnder interferometers, were fabricated based on the single line strategy using a pulse energy of  $0.34\text{ }\mu\text{J}$  and a scanning velocity of  $50\text{ }\mu\text{m/s}$ .

### 2.3. Optical waveguide characterization

The output modal profiles and waveguide losses were measured with an end-fire coupling setup seeded at two different wavelengths: 633 nm (He-Ne laser) and 800 nm (Ti-Sa laser). The Ti-Sa ring laser (0.4 cm<sup>-1</sup> linewidth) emits in continuous wave and can be tuned in the 770-920 nm spectral range. Light injection was done by focusing the beams with a 10× (0.25 NA) microscope objective, and the output modal profiles (near-field) were imaged onto a CMOS camera (IDS uEye SE) through a 20× (0.40 NA) microscope objective. A flip-mirror allows the alternative use of other diagnosis elements as a power-meter or a spectrometer. Particularly, fluorescence emitted from the optical waveguides was measured by blocking the injected light with a long pass filter and locating the tip of an optical fiber connected to a mid-IR spectrometer (Hamamatsu C9913GC) at the focal plane of MO2 (see Fig. 2). Linear polarizers and half-wave plates were used to control both the input light polarization and the input power. When required, a white-light LED was used to illuminate the sample through the input microscope, thus obtaining microscopic pictures of the waveguide outputs: this technique is very useful to identify the guiding region in the laser modified track. To analyze propagation loss, we used the scattered-light method [17] by imaging the longitudinal section of the coupled waveguide onto another CMOS camera (IDS uEye SE). From the pictures, the decay of the transmitted power along the waveguide could be extracted.

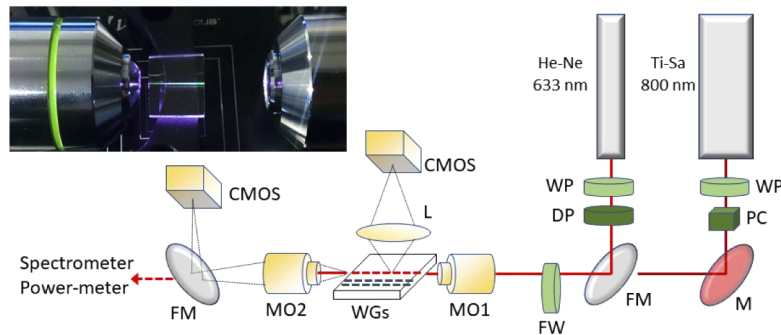


**Fig. 2.** Setup for waveguide characterization. WP: half-wave plate, PC: polarizing cube, DP: dichroic polarizer, M: mirror, FM: flip mirror, MO: microscope objective, FW: filter wheel, L: lens ( $f=20$  mm). The inset shows the up-conversion from a straight waveguide injected with 800 nm light.

### 2.4. Refractive index contrast

From the modal profiles of the waveguides, we reconstructed the refractive index profiles by using the inverse Helmholtz technique [18]. The noise of the pictures was reduced by applying a Gaussian filter, and then the index profile was estimated from the intensity distributions  $I(x, y)$  with the expression:

$$\Delta n(x, y) \cong \frac{\nabla^2 A(x, y)}{2nk^2 A(x, y)} \quad (1)$$

where  $A(x, y) \sim \sqrt{I(x, y)}$ ,  $n$  is the refractive index of the unprocessed material at the incident wavelength  $\lambda$  ( $n_{633}=1.5339$  and  $n_{800}=1.5294$ ), and  $k = 2\pi/\lambda$ . The index contrast is taken as the maximum range of  $\Delta n$  obtained in the guiding area.

### 3. Results and discussion

#### 3.1. Single line waveguides

All the irradiation conditions that we tested for the inscription of the single line scans with pulse energy equal or above to  $0.17 \mu\text{J}$ , lead to light confinement both in the visible (633 nm) as in the near infrared (800 nm). We will focus the attention in the results for the near infrared due to interest of the waveguides as active elements operating in this spectral range. In Fig. 3 we summarize some of the results obtained for that wavelength in single line waveguides. The first column (Fig. 3(a)) corresponds to the near-field intensity profiles at 800 nm of the waveguides fabricated with three different pulse energies,  $0.17 \mu\text{J}$ ,  $0.34 \mu\text{J}$  and  $0.68 \mu\text{J}$ , and the minimum scanning velocity ( $20 \mu\text{m/s}$ ). In the three cases the waveguides behave as single mode at 800 and 633 nm and show very good confinement. The insets show the microscopic pictures of the waveguides cross section. At the highest energy severe damage is evident at the track, but light guiding is still observed at the tip of the track, and for this reason the modal profile has no radial symmetry and shows a dip in the upper part. The effect of increasing the scanning velocity (not shown in the figure) was a worse light confinement and a degradation of the modal profiles, although even at  $250 \mu\text{m/s}$  the lines inscribed with the three energies behave as waveguides.

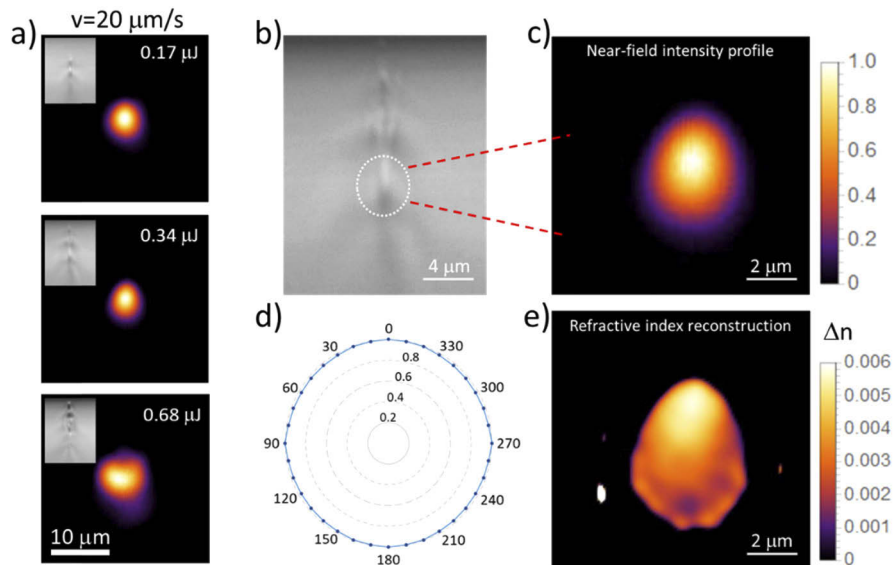


**Fig. 3.** a) Normalized near-field modal profiles (800 nm) of single line waveguides fabricated with writing conditions as indicated. Inset: microscopic pictures of the waveguides. b) Enlarged view of the waveguide cross-section ( $20 \mu\text{m/s}$ ,  $0.34 \mu\text{J/pulse}$ ) indicating the guiding region. c) Near-field modal profile. d) All-angle polarization dependence of the waveguide transmission. e) Laser-induced refractive-index reconstruction.

The best results obtained in terms of propagation loss were obtained for the waveguides fabricated with  $0.34 \mu\text{J}$  pulse energy and  $20 \mu\text{m/s}$  scanning velocity:  $1.7 \pm 0.3 \text{ dB/cm}$  at 633 nm, and  $1.9 \pm 0.4 \text{ dB/cm}$  at 800 nm. For the calculation of these values it was taken into account the absorption of the sample at the respective wavelength due to the presence of the doping ions in the glass. Increasing the scanning velocity for waveguide fabrication had the effect of an important increase in propagation loss, as expected from the worse confinement:  $5.0 \pm 1.0 \text{ dB/cm}$  (633 nm) and  $4.1 \pm 0.8 \text{ dB/cm}$  (800 nm).

Our results cannot be compared with the previous work on waveguides fabricated in RE doped oxyfluoride GC [11] provided that the propagation loss was not reported in that paper.

Concerning the studies performed in oxyfluoride glass [19], the comparison is not direct provided that the reported value of the optimized case (3.2 dB/cm) was measured at 1550 nm.

The enlarged picture of the waveguide cross section and modal profile corresponding to the best result in terms of loss (20  $\mu\text{m/s}$ , 0.34  $\mu\text{J/pulse}$ ) can be seen in Fig. 3(b) and (c), where the guiding region is marked with the white circle in the lower part of the track. The dependence of the propagation loss with the input laser polarization was also studied in this case, showing almost no dependence as it can be seen in the polar plot of Fig. 3(d), what is very interesting for the operation of the waveguides as amplifying elements. From the modal profile (Fig. 3(c)) we extracted the refractive index modification in the guiding region (Fig. 3(e)), leading to a maximum refractive index increase of  $\sim 6 \cdot 10^{-3}$ . This value is twice the refractive index increase reported in [11] for the waveguides fabricated in oxyfluoride GC in the high-repetition rate regime.

In the range of energies in which light guiding has been found ( $\geq 0.17 \mu\text{J}$ ), the laser damage tracks consist of non-uniform structures with a strongly damaged zone (dark region in the upper part of Fig. 3(b)) followed by a narrow and smoother track (bright region in the middle of Fig. 3(b)). This kind of structure, with an elongated shape along the pulse propagation direction even though the beam was focused by a large numerical aperture lens, evidences the dynamics of non-linear filamentary propagation [20] near the focal region.

The waveguide is formed in the region of weak modification under the strongly damaged area (see dotted circle in Fig. 3(b)). However, we have not been able to find light confinement in the laser tracks produced with a pulse energy smaller than 0.17  $\mu\text{J}$ , for which no optical breakdown is produced and only weak modification appears (pictures not shown). It means that severe damage is required to produce a significant refractive index increase near the strongly affected region able to produce light confinement. On the other hand, the modal profile (Fig. 3(c)) and the refractive index reconstruction (Fig. 3(e)), are spatially wider than the light region of the weak damage track: the mode is highly symmetrical and does not follow the elongated shape of the track. Then, we think that, in addition to the modification directly induced in the GC by the laser pulse in the guiding region, the stress created in the highly damaged part of the track may contribute to increase the refractive index in this region. This effect of guiding at the tips of a strongly damaged region is very usual in crystalline materials (see for instance [21]).

### 3.2. Multiscan, double-line and cladding waveguides

The technique of multiscan for waveguide fabrication [14] allows the shaping of the refractive index profiles, thus controlling the modal behavior of the waveguide (monomode/multimode), extending the operation spectral region to longer wavelengths [22] and, in some cases, reducing the propagation loss of the waveguide [23]. The typical strategy consists of using a lateral separation between consecutive scans smaller than the transverse size of the track (less than 1  $\mu\text{m}$ ), thus requiring a very large number of laser scans, increasing a lot the processing time. In our study, we pursued the possibility to produce the shaping of the modal behavior but trying to keep reasonably low the processing time for a single waveguide. For that reason, we used a considerably large separation between adjacent tracks (2  $\mu\text{m}$ ) in order to enlarge laterally the refractive index modification to about 7-8  $\mu\text{m}$  (see inset in Fig. 4(a)). In this case we obtained a multimodal waveguide at 633 nm ( $\text{TE}_{20}$  shown in Fig. 4(a), column on the left) and a single mode with horizontally stretched profile at 800 nm (Fig. 4(a), column on the right). The propagation loss did not improve the value reported for the single-line waveguide, but we got the desired control of the mode.

On the other hand, the fabricated double-line structures did not produce light guidance between the damage tracks neither in the visible nor in the near infrared, even though the pulse energy used for fabrication was increased up to the  $\mu\text{J}$  level. Light is confined mainly at the ends of the damage tracks and only a residual component remains in the central region (results not shown in the figure), suggesting that the refractive index increase that could be created due to local

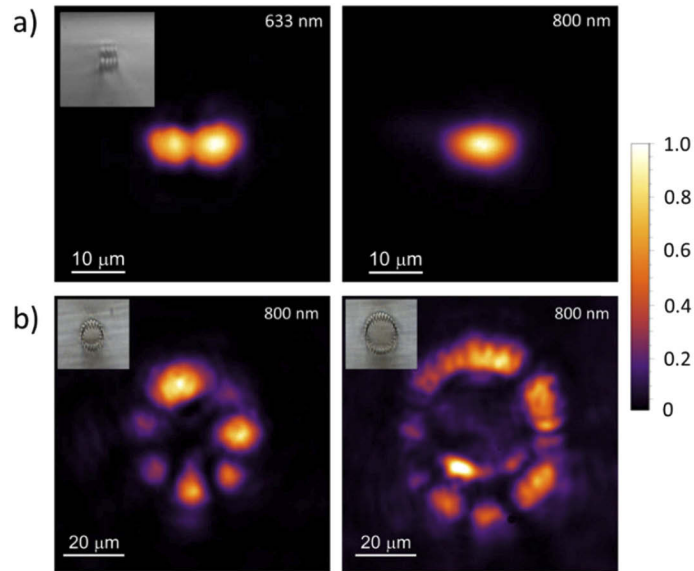


**Fig. 4.** a) Normalized near-field modal profiles (633 nm and 800 nm) corresponding to multi-scan waveguides fabricated with 0.17  $\mu\text{J}$  at 50  $\mu\text{m}/\text{s}$ . Inset: microscopic picture of the waveguide cross-section. b) Normalized near-field modal profiles (800 nm) of cladding waveguides (radius 10  $\mu\text{m}$  and 15  $\mu\text{m}$ ) fabricated with 0.34  $\mu\text{J}$  at 250  $\mu\text{m}/\text{s}$ . Inset: microscopic pictures of the waveguides cross-section.

compression in the region between both laser scans has smaller magnitude than the increase produced directly at the laser tracks.

Finally, the circular-cladding structures lead to light confinement mainly in the cladding region for 800 nm wavelength (profiles shown in Fig. 4(b)) for the two radii, 10 and 15  $\mu\text{m}$ , evidencing the fact that cladding exhibits an enhanced refractive index. Only some guidance appears in the core (Fig. 4(b), right panel), at the neighborhood of the tracks, that may be due to residual stress created near the cladding. At 633 nm, no guidance at all is produced probably due to the presence of damage at the tracks.

### 3.3. 3D photonic devices

To address the suitability of the glass as substrate for the integration of complex photonic elements, we implemented several splitter designs both 2D as 3D (see the sketch in Fig. 5, column on the left) using a pulse energy of 0.34  $\mu\text{J}$  and a scanning velocity of 50  $\mu\text{m}/\text{s}$ . The modal profiles at output preserved the single mode behavior at 633 and 800 nm (see normalized intensity for 800 nm in Fig. 5, central column). In the 1 $\times$ 2 splitter and MZ interferometer the modes are very well confined although in the 1 $\times$ 4 cases (2D and 3D) some spurious light appears out of the waveguide core, probably due to radiation in the secondary splitting transition of the structure.

The splitting losses were estimated by comparing the total output power (adding the power at the output of each of the 2/4 arms,  $P_i$ ) with the output power of a straight waveguide fabricated under the same irradiation conditions ( $P_0$ ):

$$\eta = -10 \cdot \log_{10} \left( \frac{\sum_i P_i}{P_0} \right) \quad (2)$$

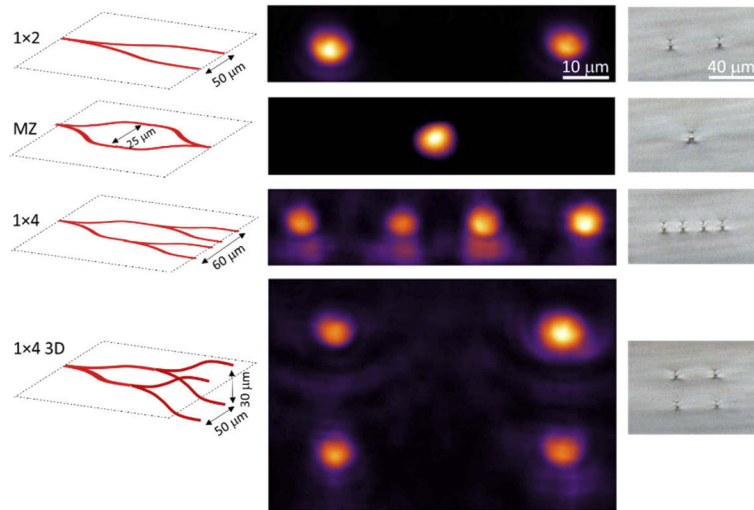


**Fig. 5.** Schematics of the implemented photonic elements (column on the left), normalized near-field modal profiles at 800 nm (central column), and microscopic pictures of the output facet (column on the right). From top to bottom, 1×2 splitter, Mach-Zehnder interferometer, 1×4 splitter (2D), and 1×4 splitter (3D).

Results are shown in Table 1. The splitting ratios can be tuned by slight changes in the position of light coupling at the entrance of the waveguide, but precise equalization between the waveguides output was not always possible in 1×4 structures, probably due to some asymmetry created during the laser writing process.

**Table 1. Additional losses of complex devices at 800 nm (losses in dB)**

1×2	MZ	1×4 (2D)	1×4 (3D)
2.0	4.0	3.7	4.4

### 3.4. Fluorescence measurements

The near infrared emission spectrum of the  $\text{Er}^{3+}/\text{Yb}^{3+}$  co-doped sample was obtained in the 900-1700nm spectral range by exciting with  $\sim 800$  nm light. By tuning the incident wavelength of the CW Ti:Sa laser, we were able to detect a strong on-axis co-propagating fluorescence signal excited during the pump propagation in the waveguide. Figure 6 shows the fluorescence spectrum for the  $\text{Er}^{3+}/\text{Yb}^{3+}$  co-doped GC sample obtained by exciting at 800 nm in resonance with the  $^4\text{I}_{9/2}$  ( $\text{Er}^{3+}$ ) level. After excitation of this level, the next lower levels are populated by multi-phonon relaxation. The spectrum shows, in addition to the  $\text{Er}^{3+}$  emissions, corresponding to the  $^4\text{I}_{11/2} \rightarrow ^4\text{I}_{15/2}$  and  $^4\text{I}_{13/2} \rightarrow ^4\text{I}_{15/2}$  transitions the one corresponding to the  $^2\text{F}_{5/2} \rightarrow ^2\text{F}_{7/2}$  transition of  $\text{Yb}^{3+}$ . The presence of the  $\text{Yb}^{3+}$  emission around 1000 nm indicates that an energy transfer from  $\text{Er}^{3+}$  to  $\text{Yb}^{3+}$  ions takes place. When the pump power output of the laser approaches 100 mW, a visible green-yellow up-conversion can be observed along the waveguide as shown in the inset of Fig. 2.

It is worthy to mention that the on-axis co-propagating fluorescence excited in the waveguide, shown in Fig. 6, exhibits the same spectral features as those obtained by exciting the bulk GC [10], which demonstrates that, in the waveguide region, there is no significant influence of the laser writing process on the GC nanostructure.



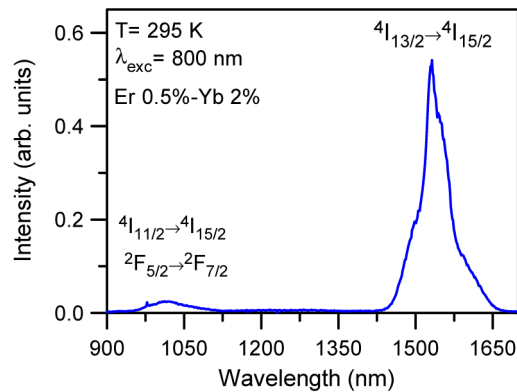


Fig. 6. Fluorescence signal recorded on-axis at the output of the waveguide.

#### 4. Conclusions

We have demonstrated the fabrication of 3D optical waveguides in  $\text{Er}^{3+}/\text{Yb}^{3+}$  oxyfluoride nano-glass ceramics by femtosecond laser pulses in the low repetition-rate regime (1 kHz). The fabrication is not critical, finding a wide range of irradiation conditions (pulse energy and scanning velocity) in which guiding structures are produced, supporting high-quality modes. The optimum parameters in terms of propagation loss were found to be  $0.34 \mu\text{J}/\text{pulse}$  and a scanning velocity of  $20 \mu\text{m}/\text{s}$  scanning velocity, for which a value of  $1.9 \pm 0.4 \text{ dB}/\text{cm}$  was measured at 800 nm. Under these conditions, the refractive index increase produced in the waveguide was  $\sim 6 \cdot 10^{-3}$ . The technique of multi-scan inscription was successfully applied to tailor the refractive index profile of the waveguides, obtaining multimodal structures. Concerning the active operation of the waveguides, fluorescence of the  $\text{Er}^{3+}/\text{Yb}^{3+}$  was detected on-axis by seeding the waveguides at  $\sim 800 \text{ nm}$  in resonance with the  $^4\text{I}_{9/2}$  ( $\text{Er}^{3+}$ ) level. These results, together with the possibility to produce 3D Y-splitters demonstrated in our work, suggest that this material is an excellent host for the integration of 3D active photonic circuits by direct femtosecond laser irradiation.

#### Funding

Ministerio de Economía y Competitividad (FIS2017-87970R, MAT2017-87035-C2-1-P/-2-P); Consejería de Educación, Junta de Castilla y León (SA287P18); Euskal Herriko Unibertsitatea (GIU17/014); Eusko Jaurlaritz (PIBA2018-24).

#### Disclosures

The authors declare no conflict of interest.

#### References

1. K. M. Davis, K. Miura, N. Sugimoto, and K. Hirao, "Writing waveguides in glass with a femtosecond laser," *Opt. Lett.* **21**(21), 1729–1731 (1996).
2. S. Gross and M. J. Withford, "Ultrafast-laser-inscribed 3D integrated photonics: challenges and emerging applications," *Nanophotonics* **4**(3), 332–352 (2015).
3. R. Osellame, G. Cerullo, and R. Ramponi, *Femtosecond Laser Micromachining: Photonic and Microfluidic Devices in Transparent Materials* 123, (Springer Science & Business Media, 2012).
4. C. B. Schaffer, J. F. García, and E. Mazur, "Bulk heating of transparent materials using a high-repetition-rate femtosecond laser," *Appl. Phys. A* **76**(3), 351–354 (2003).
5. R. R. Thomson, A. K. Kar, and J. Allington-Smith, "Ultrafast laser inscription: an enabling technology for astrophotonics," *Opt. Express* **17**(3), 1963–1969 (2009).
6. R. Osellame, V. Maselli, R. Martínez, R. Ramponi, and G. Cerullo, "Integration of optical waveguides and microfluidic channels both fabricated by femtosecond laser irradiation," *Appl. Phys. Lett.* **90**(23), 231118 (2007).

7. M. Ams, G. D. Marshaall, P. Dekker, J. A. Piper, and M. Withford, "Ultrafast laser written active devices," *Laser Photonics Rev.* **3**(6), 535–544 (2009).
8. A. de Pablos-Martín, M. Ferrari, M. Pascual, and G. Righini, "Glass-ceramics: a class of nanostructured materials for photonics," *Rivista del Nuovo Cimento* **38**(7), 311–369 (2015).
9. E. Soares de Lima Filho, K. Venkata Krishnaiah, Y. Ledemi, Y.-J. Yu, Y. Messaddeq, G. Nemova, and R. Kashyap, "Ytterbium-doped glass-ceramics for optical refrigeration," *Opt. Express* **23**(4), 4630–4640 (2015).
10. G. Gorni, R. Balda, J. Fernández, L. Pascual, A. Durán, and M. J. Pascual, "Effect of the heat treatment on the spectroscopic properties of  $\text{Er}^{3+}$ - $\text{Yb}^{3+}$ -doped transparent oxyfluoride nano-glass-ceramics," *J. Lumin.* **193**, 51–60 (2018).
11. Y.-L. Wong, D. Furniss, V. Tikhomirov, E. Romanova, M. Dubov, T. Allsop, V. Mezentsev, I. Bennion, T. Benson, and A. Seddon, "Femtosecond laser writing of buried waveguides in Erbium-doped oxyfluoride glasses and nano-glass-ceramic," in *10th Anniversary International Conference On Transparent Optical Networks (2008)*, pp. 234–238.
12. G. Gorni, J. J. Velázquez García, G. C. Mater, and A. Duran, "Selective excitation in transparent oxyfluoride glass-ceramics doped with  $\text{Nd}^{3+}$ ," *J. Eur. Ceram. Soc.* **37**(4), 1695–1706 (2017).
13. C. Florea and K. A. Winick, "Fabrication and characterization of photonic devices directly written in glass using femtosecond laser pulses," *J. Lightwave Technol.* **21**(1), 246–253 (2003).
14. Y. Nasu, M. Kohtoku, and Y. Hibino, "Low-loss waveguides written with a femtosecond laser for flexible interconnection in a planar light-wave circuit," *Opt. Lett.* **30**(7), 723–725 (2005).
15. J. Burghoff, S. Nolte, and A. Tünnermann, "Origins of waveguiding in femtosecond laser-structured  $\text{LiNbO}_3$ ," *Appl. Phys. A* **89**(1), 127–132 (2007).
16. A. G. Okhrimchuk, A. V. Shestakov, I. Khrushchev, and J. Mitchell, "Depressed cladding, buried waveguide laser formed in a  $\text{YAG:Nd}^{3+}$  crystal by femtosecond laser writing," *Opt. Lett.* **30**(17), 2248–2250 (2005).
17. Y. Okamura, Sh. Yoshinaka, and S. Yamamoto, "Measuring mode propagation losses of integrated optical waveguides: a simple method," *Appl. Opt.* **22**(23), 3892–3894 (1983).
18. L. Mccaughan and E. Bergmann, "Index distribution of optical waveguides from their mode profile," *J. Lightwave Technol.* **1**(1), 241–244 (1983).
19. R. R. Thomson, S. Campbell, I. J. Blewett, A. K. Kar, D. T. Reid, S. Shen, and A. Jha, "Active waveguide fabrication in erbium-doped oxyfluoride silicate glass using femtosecond pulses," *Appl. Phys. Lett.* **87**(12), 121102 (2005).
20. L. Sudrie, A. Couairon, M. Franco, B. Lamouroux, B. Prade, S. Tzortzakis, and A. Mysyrowicz, "Femtosecond laser-induced damage and filamentary propagation in fused silica," *Phys. Rev. Lett.* **89**(18), 186601 (2002).
21. V. Apostolopoulos, L. Laversenne, T. Colomb, C. Depeursinge, R. Salathe, M. Pollnau, R. Osellame, G. Cerullo, and P. Laporta, "Femtosecond-irradiation-induced refractive-index changes and channel waveguiding in bulk  $\text{Ti}^{3+}$ :Sapphire," *Appl. Phys. Lett.* **85**(7), 1122–1124 (2004).
22. J. Martínez, A. Ródenas, T. Fernández, J. R. Vázquez de Aldana, R. Thomson, M. Aguiló, A. Kar, J. Solís, and F. Díaz, "3D laser-written silica glass step-index high-contrast waveguides for the 3.5  $\mu\text{m}$  mid-infrared range," *Opt. Lett.* **40**(24), 5818 (2015).
23. R. R. Thomson, H. T. Bookey, N. Psaila, S. Campbell, D. T. Reid, S. Shen, A. Jha, and A. K. Kar, "Internal gain from an erbium-doped oxyfluoride-silicate glass waveguide fabricated using femtosecond waveguide inscription," *IEEE Photonics Technol. Lett.* **18**(14), 1515–1517 (2006).